



**HAL**  
open science

## Line-shape parameters for the first rotational lines of HD in He

Franck Thibault, Raúl Z Martínez, Dionisio Bermejo, Piotr Wcislo

► **To cite this version:**

Franck Thibault, Raúl Z Martínez, Dionisio Bermejo, Piotr Wcislo. Line-shape parameters for the first rotational lines of HD in He. *Molecular Astrophysics*, 2020, 19, pp.100063. 10.1016/j.molap.2020.100063 . hal-02572410

**HAL Id: hal-02572410**

**<https://univ-rennes.hal.science/hal-02572410>**

Submitted on 13 May 2020

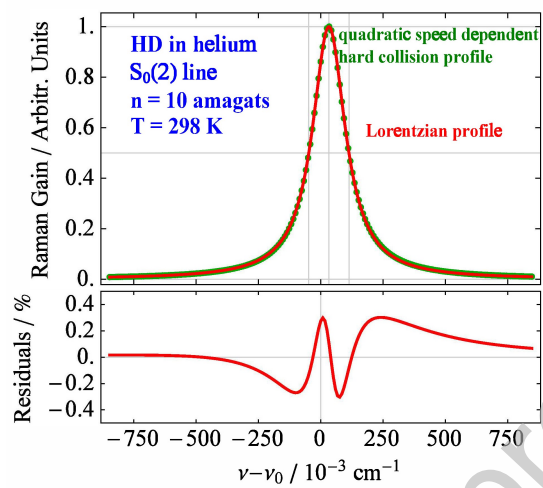
**HAL** is a multi-disciplinary open access archive for the deposit and dissemination of scientific research documents, whether they are published or not. The documents may come from teaching and research institutions in France or abroad, or from public or private research centers.

L'archive ouverte pluridisciplinaire **HAL**, est destinée au dépôt et à la diffusion de documents scientifiques de niveau recherche, publiés ou non, émanant des établissements d'enseignement et de recherche français ou étrangers, des laboratoires publics ou privés.

**Highlights**

- Close-coupling values of pressure broadening and shift coefficients for HD in He
- Close-coupling values of the complex Dicke parameters
- Line shape parameters of purely rotational R(j=0-3) and S(j=0-3) lines
- Application of the generalized Hess method for beyond Voigt profiles
- Experimental data for the rotational Raman S lines

## Graphical abstract



# Line-shape parameters for the first rotational lines of HD in He

Franck Thibault\*

*Univ Rennes, CNRS, IPR (Institut de Physique de Rennes)-UMR 6251, F-35000 Rennes, France*

Raúl Z. Martínez, Dionisio Bermejo

*Instituto de Estructura de la Materia, IEM-CSIC. Serrano, 123. 28006 Madrid, Spain*

Piotr Wcisło

*Institute of Physics, Faculty of Physics, Astronomy and Informatics, Nicolaus Copernicus University, Grudziadzka 5, 87-100 Torun, Poland*

---

## Abstract

We report theoretical and experimental line-shape parameters for He-perturbed pure rotational HD lines that are relevant for the studies of gas giants atmospheres. Besides the usual pressure broadening and shift parameters, we also report their speed dependencies and Dicke parameters. The theoretical values, obtained from quantum dynamical calculations, are for the R( $j=0-3$ ) lines and S( $j=0-2$ ) and temperatures from 10 to 500 K. The measurements, performed using stimulated Raman spectroscopy, were done for the S( $j=0-2$ ) rotational Raman lines at 77, 195 and 298 K. We also compare the results of our calculations with pressure broadening and line shift coefficients available in the literature at 77, 195 and 300 K for the studied R lines. We demonstrate that a simple Voigt profile is insufficient to accurately model the shapes of He-perturbed HD lines at conditions relevant to gas giants atmospheres, and one should incorporate also the speed-dependent effects and velocity-changing collisions.

*Keywords:* H<sub>2</sub>, He, HD, pressure broadening, line shift, Dicke parameters

---

*Email address:* [franck.thibault@univ-rennes1.fr](mailto:franck.thibault@univ-rennes1.fr) (Franck Thibault\*)

\*Corresponding author

---

## 1. Introduction

The deuterium hydride molecule (also known as the hydrogen deuteride molecule) is of great importance for astrophysics and planetology (Tennyson 2003; Encrenaz et al. 2004; Menten and Wyrowski 2011). The measurement of the D/H ratio is fundamental for understanding the evolution of the Universe from the standard Big Bang nucleosynthesis as well as for understanding the delivery of water to Earth's oceans (Altwegg et al. 2015). Since molecular hydrogen is the major constituent element of the giant planets the relative HD abundance is well suited to determine this ratio. The Herschel onboard PACS (Photodetector Array Camera & Spectrometer) instrument measurements of the rotational R(0) and R(1) HD lines in the atmospheres of Uranus and Neptune confirmed the deuterium enrichment in the atmospheres of these two planets compared to the protosolar value (Feuchtgruber et al. 2013). In the same spirit the R(2) and R(3) lines of HD were recorded by the Short Wavelength Spectrometer (SWS) onboard the Infrared Space Observatory (ISO) for studying the atmosphere of Saturn and Jupiter (Lellouch et al. 2001). The 120- and 5-fold enrichment of the D/H ratio on Venus and Mars compared to Earth is a fundamental constraint on models for their atmospheric evolution (Encrenaz et al. 2004).

The HD molecule is the simplest heteronuclear molecule and thus possesses a (weak) electric dipole moment. Throughout the last decade there has been a renewed interest in HD spectroscopic properties. Pachucki and Komasa (2008) calculated the electric dipole moments for the first purely rotational R lines and R and P lines of the fundamental and first 4 overtones in the electronic ground state. They later on provided (Pachucki and Komasa 2010) very accurate dissociation energies for all rotationvibrational states in the same electronic state. Meanwhile, Sprecher et al. (2010) using a hybrid experimental-theoretical method, determined the adiabatic ionization energy and the dissociation energy of HD and Kassi and Campargue (2011) provided a line list of electric dipole

30 and quadrupole transitions of the first overtone by using cavity ring down spectroscopy (CRDS). In addition, the latter study reported the transition moments of the studied lines. For both studies, the agreement with the *ab initio* calculations of Pachucki and Komasa (2010) was very good. More recently, Cozijn et al. (2018) performed sub-Doppler measurements of the frequency of the R(1) to R(3) lines of the 2-0 band of HD. The former line was also measured by Tao et al. (2018) using a comb-locked CRDS. Since the line position of these two independent measurements disagrees by 0.895 MHz, Fasci et al. (2018) remeasured it by using frequency-stabilized CRDS. Such highly accurate measurements provide benchmark data for testing non adiabatic and relativistic corrections and quantum electrodynamics for molecules and represent also a test for fundamental physics (Salumbides et al. 2013; Ubachs et al. 2016; Cozijn et al. 2018; Tao et al. 2018; Fasci et al. 2018; Wcisło et al. 2018).

In the present study we are interested in HD in helium baths. The HD-He system is the simplest interacting pair after H<sub>2</sub>-He, D<sub>2</sub>-He and T<sub>2</sub>-He. The H<sub>2</sub> molecule and its isotopologues interacting with helium have been thoroughly investigated in the last decades (for a review see Thibault et al. (2016, 2017); Wcisło et al. (2018); Martínez et al. (2018); Jwiak et al. (2018)). For instance, in view of the role played by HD in the astrophysics and astrochemistry of the interstellar media, the rovibrational quenching rate coefficients of HD in collisions with helium (Nolte et al. 2011) were calculated using Muchnick and Russek (1994) potential energy surface (PES) and the rotational rate constants were calculated more recently by Zhou and Chen (2017) using the Bakr, Smith, and Patkowski (BSP) PES (Bakr et al. 2013). Transport and second virial coefficients were also calculated for the HD-He system (Green et al. 1983; McCourt et al. 2005; Garberoglio et al. 2014).

HD is particular because its weak, non-BornOppenheimer, permanent dipole moment is of the same order as the HD-He supramolecular collision-induced dipole moment. Thus HD, and in particular HD in He, were studied to investigate collision-induced effects in allowed rotational or rovibrational spectra of HD (Tabisz 2003). A first effect, the so-called intracollisonal effect, is due

to an interference between the permanent dipole moment and the collisionally induced one. As a consequence Fano profiles were observed where one could expect to see a Lorentzian or Voigt profile for an isolated line. At higher densities (above about 50 amg) the intercollisional interference effect, due to succeeding collisions, may also contribute to the spectra. Thus the allowed lines sit on a broad collision-induced background. In the course of these studies the standard pressure broadening and shift coefficients of the first pure rotational lines were measured at 77, 195 and 295 K (Drakopoulos and Tabisz 1987; Ulivi et al. 1989; Lu et al. 1993). More recently, Gustafsson and Frommhold (2001a,b) revisited this problem using the radiative close coupling theory where only binary collisions are accounted for. Starting from a dipole-moment surface for HD-He and the HD permanent dipole moment, these authors generated fully *ab initio* the spectral regions around the purely rotational  $R_0(0)$  and  $R_0(1)$  lines as well as the region around the  $R_1(0)$  line of the fundamental band at 77 K. It should be noted that the interference mechanism should also manifest itself in a Raman spectrum when a permanent and an interaction-induced polarizability interfere.

In this article we present the generalized spectroscopic cross sections obtained from close coupling dynamical calculations performed on the most recent *ab initio* PES (Thibault et al. 2017) which is an improved version of the original BSP PES (Bakr et al. 2013). Following the generalized Hess method (GHM) of Monchick and Hunter (1986) we obtained, from these cross sections and the related collision integrals, line shape parameters for the  $R_0(j=0-3)$  and  $S_0(j=0-2)$  lines for various temperatures between 10 and 500 K. Such parameters may be implemented in standard Lorentzian, Dicke and Voigt profiles and more sophisticated ones such as Hess (Hess 1972), Pine (Pine 1999), Hartmann-Tran (Tennyson and et al. 2014), the speed dependent billiard-ball profile of Ciurylo et al. (2001) and Blackmore profiles (Blackmore 1987; Wciso and Ciuryo 2013) (for a review of different profiles see Hartmann et al. (2008, 2018)). In addition, we present the first measurements for the above mentioned pure rotational Stokes lines of HD in helium baths at 77, 195 and 298 K. We show that theoretical data alone, such as collisional pressure broadening and pressure-induced

line shift coefficients, are not sufficient to match the experimental data. Our raw data are carefully analysed using a speed dependent hard collision profile based on our *ab initio* calculations. We then obtain a good agreement with the measured values.

In Section 2 we briefly describe our quantum dynamical calculations. In Section 3 we illustrate the kinetic energy dependence of selected cross-sections and compare them with available data in the literature. Section 4 presents the pressure broadening and shift parameters and the complex Dicke parameters. Comparisons with experimental or theoretical data when available are also performed. The experimental part is described in section 5. In Section 6 we perform our line shape analysis which provides a direct comparison with the experimental data. We show that a proper interpretation of experimental data requires to take into account the beyond Voigt line-shape effects: speed dependence of the broadening and shift and velocity-changing collisions. Section 7 concludes the present article.

## 2. Dynamical calculations

Since, within the BornOppenheimer approximation the HD-He interaction is the same as the H<sub>2</sub>-He one, we made use of the extended and improved, by Thibault et al. (2017), original BSP PES (Bakr et al. 2013). This PES is expected to be the most accurate H<sub>2</sub>-He PES to date (Garberoglio et al. 2014; Thibault et al. 2016, 2017; Jwiak et al. 2018). The 3-dimensional H<sub>2</sub>-He PES  $V(r,R,\theta)$ , where  $r$  is the intramolecular H-H distance,  $R$  is the distance of the H<sub>2</sub> centre of mass to the helium atom and  $\theta$  the angle between them, has been adapted to the HD-He interaction by shifting the centre of mass by  $\frac{r}{6}$  thus allowing the redefinition of the Jacobi coordinates  $R$  and  $\theta$  for each geometrical configurations. The HD-He PES has been expanded over 7 Legendre polynomials  $P_L(\cos\theta)$ , with  $L$  ranging from 0 to 6 (in contrast to the H<sub>2</sub> and D<sub>2</sub> homonuclear isotopologues, for the heteronuclear HD molecule both even and

120 odd terms are required due to its lower symmetry):

$$V(r, R, \theta) = \sum_L V_L(r, R) P_L(\cos \theta). \quad (1)$$

For such light systems and at least to study purely rotational lines it is important (Schaefer and Monchick 1992; Dubernet and Tuckey 1999; Thibault et al. 2016, 2017; Martínez et al. 2018; Jwiak et al. 2018) to take into account the effect of the centrifugal distortion, thus the final radial coupling potential terms were  
125 evaluated following the same method as in Thibault et al. (2016):

$$V_{L, v_j, v'_{j'}}(R) = \int_0^\infty \chi_{v'_{j'}}(r) V_L(r, R) \chi_{v_j}(r) dr, \quad (2)$$

where  $\chi_{v_j}(r)$  designates a radial wavefunction of the rovibrational Hamiltonian of the diatomic. We set  $v = v' = 0$  for studying pure rotational transitions. Since our rotational basis was limited to  $j = 7$ , we are left with (a maximum of) 252 coupling terms. Disregarding the centrifugal distortion by setting  $j =$   
130  $j' = 0$  limits the number of radial coupling terms to 7.

Quantum dynamical calculations were done using the MOLSCAT code (Hutson and Green 1995) in conjunction with the hybrid modified log-derivative Airy propagator of Alexander and Manolopoulos (1987) for solving the close coupled equations. Propagations were carried out between 1 and 100 Å with a starting  
135 minimum step of 0.01 Å. In order to perform the thermal average of the generalized cross sections, calculations were performed for a number of relative kinetic energies from 0.1 to about 2500 cm<sup>-1</sup> with the step size varying from 0.1 to 100 cm<sup>-1</sup>. For instance for the S<sub>0</sub>(1) and R<sub>0</sub>(0) lines calculations were performed on a grid of 295 and 345 kinetic energies respectively. The rotational energy levels  
140 are the theoretical ones of Pachucki and Komasa (2010). The masses of the deuterium hydride and helium were taken to be  $m(\text{HD}) = 3.022$  u and  $m(^4\text{He}) = 4.0026$  u.

### 3. Generalized cross sections

The close-coupling expression of the generalized cross sections is given for  
145 two diatomics (one spectroscopically active molecule infinitely diluted in a bath

of a diatomic molecule) by Monchick and Hunter (1986). They can be easily adapted to the case of a diatom-atom pair (Schaefer and Monchick 1987, 1992; Demeio et al. 1995). With the GHM (Hess 1972; Corey and McCourt 1984; Monchick and Hunter 1986) two kinds of complex cross sections are necessary. The first one, denoted  $\sigma_{\lambda=0}^q(v_i j_i v_f j_f, v_i j_i v_f j_f; E_{kin})$ , associated with a spectral line  $v_i j_i \rightarrow v_f j_f$  is identical with the standard generalized spectroscopic cross sections as obtained from the relaxation theory (Baranger 1958a,b,c; Fano 1963; Ben-Reuven 1966a,b) for the collisional line-shape parameters. Its real part provides the pressure broadening cross section (PBXS), while its imaginary part yields the pressure shift cross section (PSXS). The second cross section arising from the kinetic theory, denoted  $\sigma_{\lambda=1}^q(v_i j_i v_f j_f, v_i j_i v_f j_f; E_{kin})$ , describes the diffusion of the polarization of the spectral transition. Thus collisions reorient the angular momentum and the velocity vectors as well as changing their magnitudes. The formal expressions of the generalized cross sections are given by:

$$\sigma_{\lambda}^q(v_i j_i, v_f j_f; v_i j_i, v_f j_f; E_{kin}) = \frac{\pi}{k^2} \sum_{J_i, J_f, l, l', \bar{l}, \bar{l}'} [J_i] [J_f] ([l] [l'] [\bar{l}] [\bar{l}'])^{1/2} (i)^{-l+l'+\bar{l}-\bar{l}'} \times \begin{pmatrix} l & \bar{l} & \lambda \\ 0 & 0 & 0 \end{pmatrix} \begin{pmatrix} l' & \bar{l}' & \lambda \\ 0 & 0 & 0 \end{pmatrix} \begin{bmatrix} j_i & j_i & \bar{l} & \bar{l}' \\ j_f & l & j_f & l' \\ q & J_f & J_i & \lambda \end{bmatrix} \times \left[ \delta_{ll'} \delta_{\bar{l}\bar{l}'} - \langle v_i j_i l' | S^{J_i}(E_{t_i}) | v_i j_i l \rangle \langle v_f j_f \bar{l}' | S^{J_f}(E_{t_f}) | v_f j_f \bar{l} \rangle^* \right]. \quad (3)$$

Since they were recently discussed by Martínez et al. (2018); Jwiak et al. (2018) we briefly recall some aspects of the above equation. GHM cross sections involve  $S$ -matrix elements, obtained from the MOLSCAT code (Hutson and Green 1995) in our case, where primed variables denote postcollisional values. They are calculated at the same kinetic energy  $E_{kin}$  but at different total energies  $E_{t_i} = E_{kin} + E_{v_i j_i}$  and  $E_{t_f} = E_{kin} + E_{v_f j_f}$  where  $E_{v_i j_i}$  is the rovibrational energy of the initial level of the optical transition  $v_i j_i \rightarrow v_f j_f$  of rank  $q$  with  $q=1$  for dipolar lines and  $q=2$  for quadrupolar and depolarized Raman lines (anisotropic Raman lines).  $k$  is the wavenumber associated with the kinetic

170 energy  $\hbar^2 k^2 / 2\mu$ , where  $\mu$  is the HD-He reduced mass.  $J$  and  $l$  are the total and orbital angular momenta of the colliding pair,  $[x]$  stands for  $2x+1$ ,  $(:::)$  are  $3j$  symbols and the large bracket is a  $12j$  of second kind. The latter takes also into account the coupling of the radiation-matter interaction tensor order  $q$  and the velocity operator of rank 1 (for  $\lambda=1$ ). For short, these cross sections will be de-

175 noted by  $\sigma_\lambda^q(j_i j_f; E_{kin})$  since the vibrational quantum numbers  $v_i, v_f$  are zero for the considered lines and we are only dealing with diagonal cross sections.

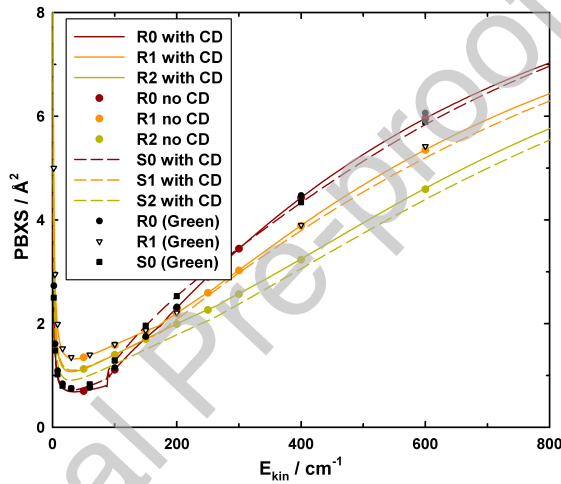


Figure 1: (Color online) Pressure broadening cross sections ( $\text{Re}\sigma_0^q(j_i j_f; E_{kin})$ ), as a function of the kinetic energy, for the  $R_0(j=0-2)$  and  $S_0(j=0-2)$  lines of HD in He. "with CD" are the results of our full calculations, taking into account the centrifugal distortion, while "no CD" are the results obtained using only 7 radial coupling terms. Black symbols represent computed values by Green (1974).

Figure 1 shows the pressure broadening cross sections (PBXS) for the  $R_0(0)$ ,  $R_0(1)$ ,  $R_0(2)$ ,  $S_0(0)$ ,  $S_0(1)$  and  $S_0(2)$  lines. First, we remark that there is almost no difference between our calculations performed with and without taking into account the centrifugal distortion (for clarity, the results of our calculations performed for S lines with no centrifugal distortion are not presented, but the same conclusions remain valid). For clarity as well, our results for the  $R_0(3)$  line are not shown. Green (1974), considering HD as a rigid rotor and using a PES

180

derived by Shafer and Gordon (1973), has computed the pressure broadening  
 185 cross sections for the  $R_0(0)$ ,  $R_0(1)$  and  $S_0(0)$  lines for collisional kinetic energies  
 between 2 and 600  $\text{cm}^{-1}$ . In Fig. 1, we compare the results of our calculations  
 with those of Green (see Table 3 of Green (1974)). They are in surprisingly  
 good agreement with our data. Pressure broadening cross sections for IR R  
 lines and Raman S lines arise both from elastic (including reorienting) collisions  
 190 and inelastic collisions. The latter contribution differs for the two types of lines  
 because an  $R(j)$  lines takes into account standard inelastic cross sections out of  
 the levels  $j$  and  $j+1$ , while an  $S(j)$  lines involves inelastic cross sections out of  
 the levels  $j$  and  $j+2$ . Finally, a visual comparison of our cross sections for the  
 $R_0(0)$  and  $R_0(1)$  lines with the ones reported in figures 3a and 4a of Schaefer  
 and Monchick (1987) shows what seems to be a very good agreement.

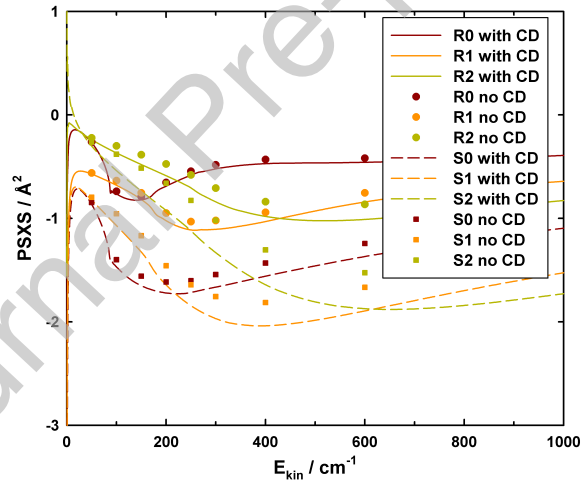


Figure 2: (Color online) Pressure shift cross sections ( $\text{Im}\sigma_0^q(j_i j_f; E_{kin})$ ), as a function of the  
 kinetic energy, for the  $R_0(j=0-2)$  and  $S_0(j=0-2)$  lines of HD in He. "with CD" are the results  
 of our full calculations, taking into account the centrifugal distortion, while "no CD" are the  
 results obtained using only 7 radial coupling terms.

195

The corresponding pressure shift cross sections (PSXS) are plotted in Fig.  
 2, where we show the differences for the  $R_0(j=0-2)$  and the  $S_0(j=0-2)$  lines with

and without taking into account the centrifugal distortion. First, we observe that this effect is more important for the PSXS than for the PBXS, as expected from previous works (Shafer and Gordon 1973; Dubernet and Tuckey 1999; Thibault et al. 2016). Moreover, we see that the centrifugal stretching effect increases with  $j$  (as expected too). Finally, our exact values for the  $R_0(j=0)$  and  $R_0(j=1)$  lines have the same behaviour with the kinetic energy and are in very good agreement with the values of Schaefer and Monchick (see Figures 3b and 4b in Schaefer and Monchick (1987)).

The real part of the Dicke cross section (DXS) related with the Dicke narrowing effect is plotted in Fig. 3. As already found for  $H_2$  or  $D_2$  in helium (Thibault et al. 2017; Martínez et al. 2018; Jwiak et al. 2018), this cross section has a very small  $j$  dependence. This may be related to the fact that these cross sections are more highly averaged quantities as compared to the PBXS since they involve additional angular momenta (see Eq. (3)). Recall also that for structureless colliding partners the real part of the DXS reduces to a simple momentum-transfer cross section (Thibault et al. 2017).

To our knowledge the imaginary parts of the DXS were never reported for HD lines in helium baths. They were safely disregarded by Schaefer and Monchick (1992). As can be seen on Fig. 4 these cross sections are very small (even smaller than the line shift cross sections) and thus their calculations are difficult. We may encounter convergence problems and truncations errors. Nevertheless, they have, overall, a small  $j$  dependence above about  $100 \text{ cm}^{-1}$ , and these XS for  $S(j)$  and  $R(j)$  lines vary roughly similarly. Moreover, we observe a threshold resonance effect near the opening of the  $j = 1$  level (near  $90 \text{ cm}^{-1}$ ). This threshold effect is also noticeable at the same kinetic energy in Fig. 1 and 2 for the  $R_0(0)$  and  $S_0(0)$  lines and was discussed in Schaefer and Monchick (1987). Additionally, we note that the centrifugal distortion plays a minor role.

The full set of our cross sections are given as supplementary material (Thibault et al. 2019), including our results for the  $R_0(3)$  line not presented in this section.

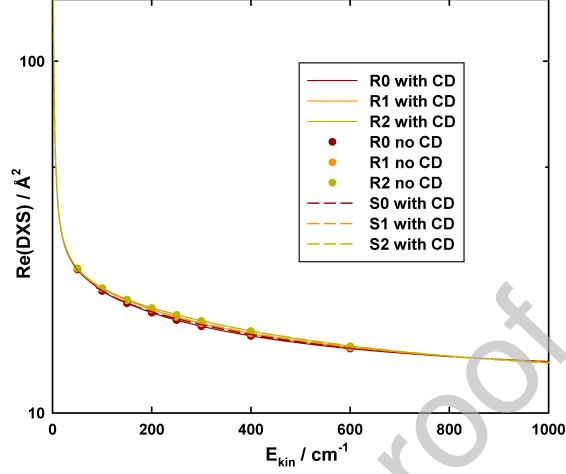


Figure 3: (Color online) Real part of the Dicke cross sections (DXS) ( $\text{Re}\sigma_1^q(j_i j_f; E_{kin})$ ), as a function of the kinetic energy, for the  $R_0(j=0-2)$  and  $S_0(j=0-2)$  lines of HD in He. "with CD" are the results of our full calculations, taking into account the centrifugal distortion, while "no CD" are the results obtained using only 7 radial coupling terms.

#### 4. Collision integrals and line shape parameters

In order to calculate the line shape parameters, it is first necessary to derive the relevant collision integrals from the generalized cross sections (Corey and McCourt 1984; Monchick and Hunter 1986; Schaefer and Monchick 1992; Demeio et al. 1995; Thibault et al. 2017; Martínez et al. 2018; Jwiak et al. 2018):

$$\omega_\lambda^{s,s'}(q) = \langle v \rangle \int dx x^{(s+s'+2)/2} e^{-x} \sigma_\lambda^q(v_i j_i; v_f j_f; E_{kin} = x k_B T) \quad (4)$$

with  $\langle v \rangle$  the mean relative speed at a given temperature  $T$ ,

$$\langle v \rangle = \sqrt{8k_B T / \pi \mu}. \quad (5)$$

and  $\mu$  is the reduced mass of the colliding pair. Then following the GHM (Hess 1972; Corey and McCourt 1984; Monchick and Hunter 1986), two collision frequencies are introduced, namely  $\omega_A$  and  $\omega_R$  (in  $\text{rad s}^{-1}$ ). The first one is the complex PB-, PS- coefficient :

$$\omega_A = n_b \omega_0^{00}(q) \equiv \Gamma - i\Delta = n_b(\gamma_0 - i\delta_0), \quad (6)$$

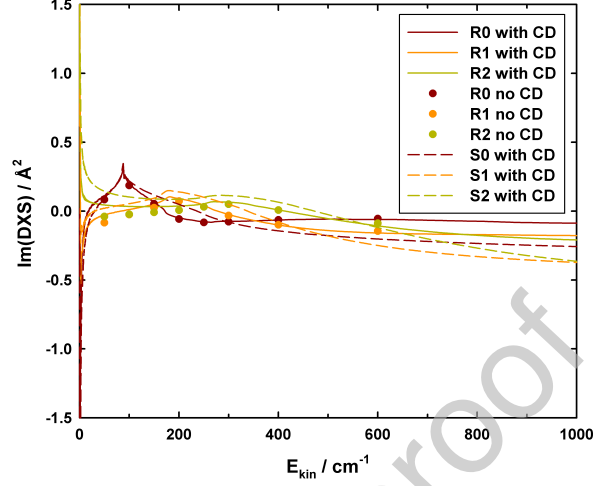


Figure 4: (Color online) Imaginary part of the Dicke cross sections (DXS) ( $\text{Im}\sigma_1^q(j_i j_f; E_{kin})$ ), as a function of the kinetic energy, for the  $R_0(j=0-2)$  and  $S_0(j=0-2)$  lines of HD in He. "with CD" are the results of our full calculations, taking into account the centrifugal distortion, while "no CD" are the results obtained using only 7 radial coupling terms.

where  $n_b$  is the number density of the perturbers, the helium atoms,  $\Gamma$  and  $\Delta$  are the usual Lorentzian collisional HWHM (half width at half maximum) and line shift, and  $\gamma_0, \delta_0$  the corresponding normalized coefficients. The second collision frequency takes into account the correlation between the translational motion and the internal changes. According to Monchick and Hunter (1986) it is expressed as a mass-weighted combination of  $\omega_1^{1,1}(q)$  and  $\omega_0^{0,0}(q)$ :

$$\omega_R = M_a \omega_A + \frac{2}{3} n_b M_b \omega_1^{1,1}(q) \quad (7)$$

with

$$M_i = \frac{m_i}{m_a + m_b}, \quad (8)$$

where  $m_a$  is the mass of the active molecule (HD) and  $m_b$  the mass of the bath particle (He); the index  $i$  stands for  $a$  or  $b$ . In the following we will call  $\omega_A$  and  $\omega_R$  the generalized Hess parameters because these are the frequencies which enter in the expression of Hess' profile (Hess 1972) with the line position  $\omega_0$  and the frequency of observation  $\omega$ .

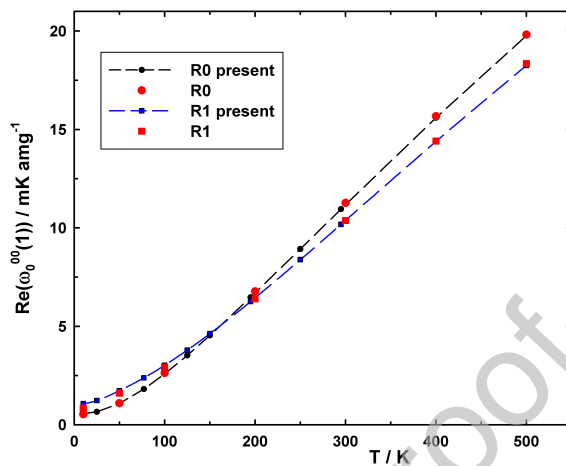


Figure 5: (Color online) Normalized (in mK/amg) real part of  $\omega_0^{0,0}(1)$  or pressure broadening coefficients as a function of the temperature. Recall that  $1 \text{ mK} = 10^{-3} \text{ cm}^{-1}$ . The red symbols represent selected data from tables 2 and 3 of Schaefer and Monchick (1992).

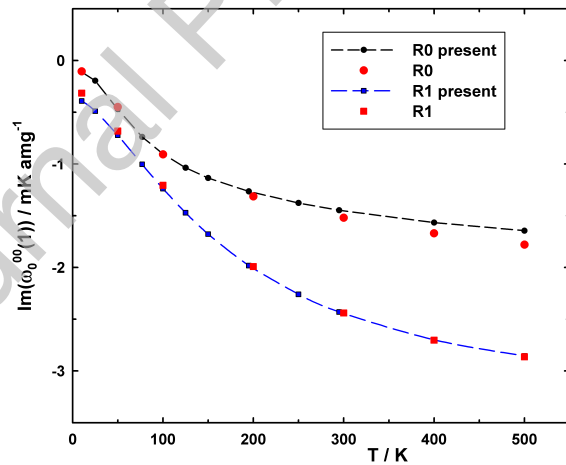


Figure 6: (Color online) Normalized (in mK/amg) imaginary part of  $\omega_0^{0,0}(1)$  or minus pressure shift coefficients as a function of the temperature. The red symbols represent selected data from tables 2 and 3 of Schaefer and Monchick (1992).

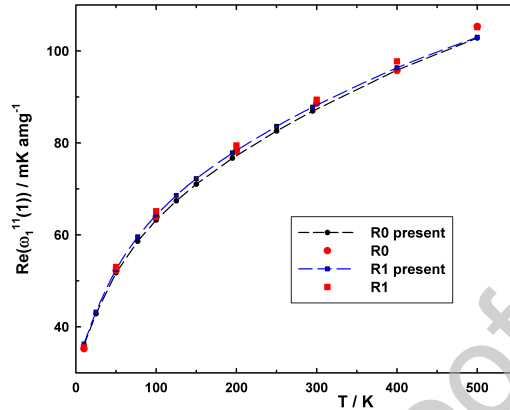


Figure 7: (Color online) Normalized (in mK/amg) real part of  $\omega_1^{1,1}(1)$  as a function of the temperature. The red symbols represent selected data from tables 2 and 3 of Schaefer and Monchick (1992).

In profiles that include the effect of the velocity changing collisions (VC) (Hartmann et al. 2008), leading to the Dicke narrowing, an effective frequency of such collisions appears. This parameter is often loosely deduced from the mass diffusion coefficient and often denoted  $\nu_{diff}$  in place of  $\nu_{opt}$ . It has been recognized by Thibault et al. (2017) that the "true" optical frequency of the VC collisions is given by the GHM as follows<sup>1</sup>:

$$\nu_{opt} = \omega_R - \omega_A. \quad (9)$$

This frequency is complex (contrary to  $\nu_{diff}$ , which is real). The discussion about the main differences between  $\nu_{diff}$  and  $\nu_{opt}$  is reported in Appendix A.

<sup>1</sup>The name optical frequency is not related to the frequency domain of an electromagnetic wave but to make the distinction with  $\nu_{diff}$  since it is  $\nu_{opt}$  that is a parameter of a line profile. To avoid confusion, this optical frequency could be named a "Generalized Hess Frequency" because it comes from Hess's theory (Hess 1972) generalized by Corey and McCourt (1984) followed by Monchick and Hunter (1986). It could also be called a "Complex Generalized Dicke Frequency", since it contains more than the usual Dicke frequency. In the end, we have settled for calling it "Complex Dicke Parameter". This is the term we use in the discussion.

Table 1: Calculated and experimental pressure broadening coefficients  $\gamma_0$  in  $10^{-3} \text{ cm}^{-1} \text{ amg}^{-1}$  for the  $R_0(j=0-3)$  lines. The  $SD_q\text{HCP}$  (for quadratic speed dependent hard collision profile) values are expected observed HWHM, see Section 6.3.

| T (K) | $R_0(0)$ | $R_0(1)$ | $R_0(2)$ | $R_0(3)$ | Ref.                             | exp./calc.       |
|-------|----------|----------|----------|----------|----------------------------------|------------------|
| 77    | 1.5      | 2.0      | 1.2      |          | Lu et al. (1993)                 | experimental     |
|       | 1.85     | 2.28     |          |          | Schaefer and Monchick (1992)     | calculations     |
|       | 1.78     | 2.32     |          |          | Gustafsson and Frommhold (2001a) | calculations     |
|       | 1.81     | 2.38     | 2.05     | 1.38     | present                          | calculations     |
|       | 1.79     | 2.36     | 2.04     | 1.37     | present                          | $SD_q\text{HCP}$ |
| 195   | 5.2      | 5.1      | 4.1      | 3.8      | Lu et al. (1993)                 | experimental     |
|       | 6.55     | 6.21     |          |          | Schaefer and Monchick (1992)     | calculations     |
|       | 6.47     | 6.26     | 5.43     | 4.06     | present                          | calculations     |
|       | 6.07     | 6.0      | 5.24     | 3.94     | present                          | $SD_q\text{HCP}$ |
| 296   |          | 11.      | 6.8      | 5.9      | Lu et al. (1993)                 | experimental     |
|       | 10.97    | 10.25    | 9.0      | 7.0      | present                          | calculations     |
|       | 10.07    | 9.62     | 8.43     | 6.67     | present                          | $SD_q\text{HCP}$ |

Figures 5, 6 and 7 compare our collision integrals with picked values<sup>2</sup> in Tables 2 and 3 of Schaefer and Monchick (1992) at various temperatures between 10 and 500 K for the  $R_0(0)$  and  $R_0(1)$  lines. We observe an overall very good agreement between these two sets of calculations.

Tables 1 and 2 provide theoretical and experimental PB- and PS- coefficients at 77, 195 and 296 K for the  $R_0(j=0-3)$  lines. When comparable, the results of our calculations are in good agreement with the radiative close coupling values of Gustafsson and Frommhold (2001a) and the CC values of Schaefer and Monchick (1992) despite that different PESs were used. On the contrary, the agreement is not satisfying with the experimental values of Tabisz and coworkers (Drakopoulos and Tabisz 1987; Ulivi et al. 1989; Lu et al. 1993), the agreement being slightly better for the shifts of the  $R_0(0)$  and  $R_0(1)$  lines. We have no

in Appendix A.

<sup>2</sup>Note that Eq. (16) of Schaefer and Monchick (1992) is incorrect: to convert the rate constant expressed in  $\text{cm}^3 \text{ s}^{-1}$  to  $\text{cm}^{-1} \text{ amagat}^{-1}$  a factor  $\frac{1}{2\pi}$  should be added.

Table 2: Calculated and experimental line shift coefficients  $\delta_0$  in  $10^{-3} \text{ cm}^{-1} \text{ amg}^{-1}$  for the  $R_0(j = 0 - 3)$  lines. The  $SD_q\text{HCP}$  (quadratic speed dependent hard collision profile) values are expected observed HWHM, see Section 6.3.

| T (K) | $R_0(0)$ | $R_0(1)$ | $R_0(2)$ | $R_0(3)$ | Ref.                             | exp./calc.       |
|-------|----------|----------|----------|----------|----------------------------------|------------------|
| 77    | 0.78     | 0.65     | -1.11    |          | Lu et al. (1993)                 | experimental     |
|       | 0.73     | 0.97     |          |          | Schaefer and Monchick (1992)     | calculations     |
|       | 0.75     | 1.04     |          |          | Gustafsson and Frommhold (2001a) | calculations     |
|       | 0.74     | 1.0      | 0.52     | 0.22     | present                          | calculations     |
|       | 0.71     | 0.98     | 0.5      | 0.2      | present                          | $SD_q\text{HCP}$ |
| 195   | 0.98     | 2.15     | 1.22     | -0.45    | Lu et al. (1993)                 | experimental     |
|       | 1.30     | 1.96     |          |          | Schaefer and Monchick (1992)     | calculations     |
|       | 1.26     | 1.98     | 1.46     | 0.89     | present                          | calculations     |
|       | 1.19     | 1.85     | 1.35     | 0.83     | present                          | $SD_q\text{HCP}$ |
| 296   |          | 2.4      | 2.8      | 1.8      | Lu et al. (1993)                 | experimental     |
|       | 1.45     | 2.45     | 2.1      | 1.5      | present                          | calculations     |
|       | 1.36     | 2.26     | 1.89     | 1.33     | present                          | $SD_q\text{HCP}$ |

clear explanation of that fact. We may suspect the quality of their spectra which  
 270 are quite noisy (see for instance Fig. 1 of Drakopoulos and Tabisz (1987) and  
 Fig. 2 of Ulivi et al. (1989)). Moreover this group used high densities (a few  
 tens of amagats) with not small mixing concentration ratios  $c_{He}/c_{HD}$ , thus the  
 contribution of the HD-HD collisions is not negligible on the widths and shifts.  
 In addition, HD-HD and HD-He interference effects affect the line shapes and  
 275 the far IR R lines are superimposed on a broad continuum due to HD-HD and  
 HD-He induced absorption. The presence of dimers is also possible at the lowest  
 temperature.

Raman spectra of the  $S_0(j=0-2)$  lines, that we report in this paper, were  
 recorded in Madrid at 77, 195 and 298 K for total densities below 1.25 amagat  
 280 and HD relative concentration smaller than 11%. Experimental details are  
 provided in the next Section. Tables 3 and 4 gather our experimental and  
 calculated values for the pure rotational Stokes lines. Here too we observe quite  
 large differences for the PB coefficients and an overall better agreement for the

Table 3: Present calculated and experimental line broadening coefficients  $\gamma_0$  in  $10^{-3} \text{ cm}^{-1} \text{ amg}^{-1}$  for the  $S_0(j = 0 - 2)$  lines. The  $SD_q\text{HCP}$  (quadratic speed dependent hard collision profile) values are expected observed HWHM, see Section 6.3.

| T (K) | $S_0(0)$ | $S_0(1)$ | $S_0(2)$ | exp./calc.       |
|-------|----------|----------|----------|------------------|
| 77    | 1.89(9)  | 2.1(1)   |          | experimental     |
|       | 1.98     | 2.12     | 1.81     | calculations     |
|       | 1.97     | 2.11     | 1.79     | $SD_q\text{HCP}$ |
| 195   | 6.1(3)   | 5.9(3)   |          | experimental     |
|       | 6.62     | 5.96     | 4.99     | calculations     |
|       | 6.28     | 5.77     | 4.86     | $SD_q\text{HCP}$ |
| 298   | 9.4(5)   | 9.4(5)   | 7.6(4)   | experimental     |
|       | 11.14    | 9.97     | 8.46     | calculations     |
|       | 10.29    | 9.37     | 8.05     | $SD_q\text{HCP}$ |

Table 4: Present calculated and experimental line shift coefficients  $\delta_0$  in  $10^{-3} \text{ cm}^{-1} \text{ amg}^{-1}$  for the  $S_0(j = 0 - 2)$  lines. The  $SD_q\text{HCP}$  (quadratic speed dependent hard collision profile) values are expected observed HWHM, see Section 6.3.

| T (K) | $S_0(0)$ | $S_0(1)$ | $S_0(2)$ | exp./calc.       |
|-------|----------|----------|----------|------------------|
| 77    | 1.75(9)  | 1.46(7)  |          | experimental     |
|       | 1.77     | 1.55     | 0.74     | calculations     |
|       | 1.71     | 1.51     | 0.71     | $SD_q\text{HCP}$ |
| 195   | 3.4(2)   | 3.1(2)   |          | experimental     |
|       | 3.32     | 3.50     | 2.38     | calculations     |
|       | 3.09     | 3.25     | 2.21     | $SD_q\text{HCP}$ |
| 298   | 3.9(2)   | 4.0(2)   | 3.0(2)   | experimental     |
|       | 4.0      | 4.63     | 3.64     | calculations     |
|       | 3.7      | 4.16     | 3.27     | $SD_q\text{HCP}$ |

shifts. We also note that the disagreement increases as temperature increases.

285 An accurate line shape analysis, trying to reconcile these two sets of data, is the object of Section 6. Data resulting from this analysis are denoted by  $SD_q\text{HCP}$  in Tables 3 - 4.

## 5. Experimental determination of the widths and shifts

The observation of the  $S_0(0)$ ,  $S_0(1)$  and  $S_0(2)$  lines of the pure rotational  
 290 Raman spectrum of HD studied in this work has been carried out through the  
 use of a high-resolution stimulated Raman spectroscopy (SRS) setup. The SRS  
 apparatus has been described in a previous article (Martínez et al. 2018) where  
 the shifting and broadening of  $D_2$  pure rotational lines were measured. The  
 modifications described therein have been kept in this work as the frequency  
 range of the studied lines is similar and temperatures are the same.

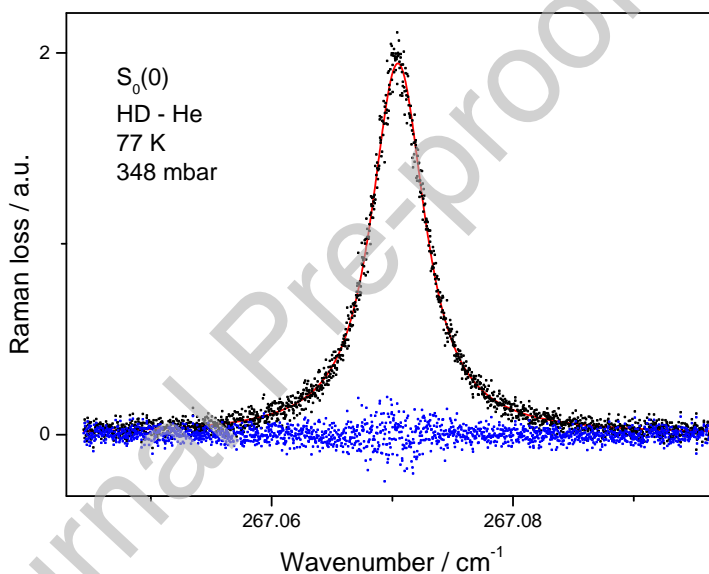


Figure 8: (Color online)  $S_0(0)$  line at 77 K. Experimental (black dots), fitted Voigt profile  
 295 (red line) and residuals (blue dots), at 348 mbar of He partial pressure.

At its core, the setup is essentially a quasi-cw pump-probe configuration in  
 which a fixed-frequency, cw laser beam acts as probe and a tunable, pulsed laser  
 beam acts as pump. The beams are spatially overlapped and focused collinearly  
 on the sample under study. To register a Raman spectrum the frequency of the  
 300 pump beam is scanned, and when the frequency difference of the two beams  
 matches that of a Raman transition an energy transfer takes place between  
 both beams. In our setup, it is detected through the intensity loss experienced

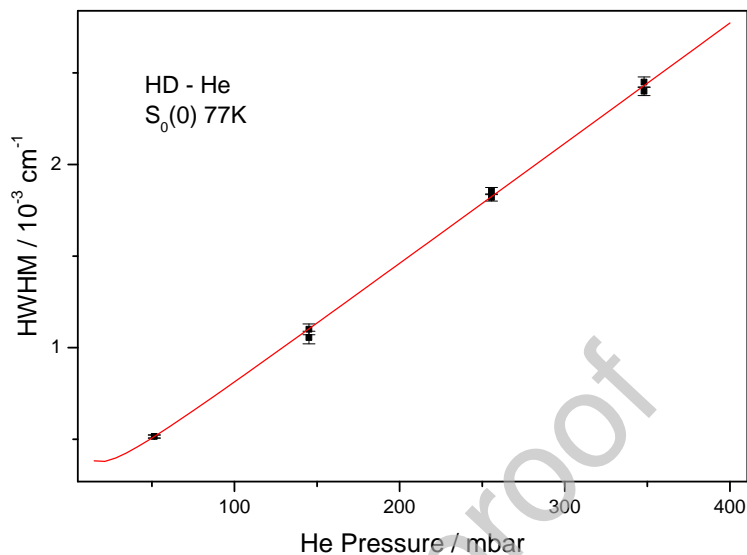


Figure 9: (Color online) Experimental line-width (HWHM) for the  $S_0(0)$  line at 77 K (black dots) and best fit to equation 3 in Martínez et al. (2018) (red line) to extract the pressure broadening coefficient.

by the high-frequency probe laser beam. Thus, by monitoring this intensity as a function of the frequency difference of the two beams a Raman spectrum of the sample is obtained. The apparatus function, which results from the convolution of the spectral profiles of the two laser beams, has a nearly Gaussian shape. The attainable resolution, loosely defined as the full width at half maximum (FWHM) of this apparatus function, is limited only by the linewidths of the two beams. This allows the recording of high resolution spectra if narrow-  
 305 linewidth lasers are employed. In the present experiment, a resolution of about  
 310  $1.8 \times 10^{-3} \text{ cm}^{-1}$  was attained.

As in the above mentioned article, perpendicular polarization of the pump and probe lasers has been used in order to make easier the separation of both lasers after interaction in the sample cell. Measurements were performed at  
 315 77, 195 and 298 K. In order to reach the first two temperatures, the body of the cell was immersed in liquid nitrogen and carbonic dry ice respectively. Every spectral line was recorded twice at four different pressures in the range

between 50 and 1000 mbar for every temperature. The HD partial pressure was kept constant, at a value between 3 and 8 mbar depending on the line and temperature, for each pressure series. The whole procedure was repeated  
320 between three and four times.

The procedure for the determination of both the line shift and line broadening coefficients was the same as described by Martínez et al. (2018): in an initial step, wavenumber corrections were applied to account for the relative  
325 thermal drift of both wavemeters (see Martínez et al. (2018) for details). Then, all the line profiles in the series were independently fitted to Voigt profiles using commercial software (Peak Fitting Module of Microcal Origin). Both the Lorentzian and Gaussian widths of the profile were initially left unconstrained, and this allowed us to verify that all the fits in each series, within the limits  
330 allowed by the experimental noise present in the spectra, converged to similar values of the Gaussian width, which also matched the width of our apparatus function. After this verification, the Gaussian width for each series was constrained to the average value obtained for the series and all the fits repeated to extract the Lorentzian contributions to the profiles. Figure 8 shows the  $S_0(0)$   
335 spectral line at 77 K and a partial He pressure of 348 mbar (black) together with the fitted Voigt profile (red) and residuals (blue) to give an idea of the quality of the fit.

The pressure broadening coefficients were obtained by fitting the lorentzian contributions extracted from the linewidths of a pressure series to Eq. (3) in  
340 Martínez et al. (2018), which consists of a linear broadening term and a nonlinear Dicke term. Figure 9 presents one example of these fits, corresponding to the  $S_0(0)$  line at 77 K. The obtained broadening coefficients are presented in Table 3 for all lines and temperatures.

A simple linear fit of the wavenumbers of the maxima against the He partial  
345 pressure in each series was used to determine the shift coefficient. Figure 10 illustrates three of these linear fits, corresponding to the  $S_0(0)$  spectral line at 77, 195 and 298 K, and gives a visual idea of the quality of the fits and the magnitude of the error bars associated to the determination of the maxima. The

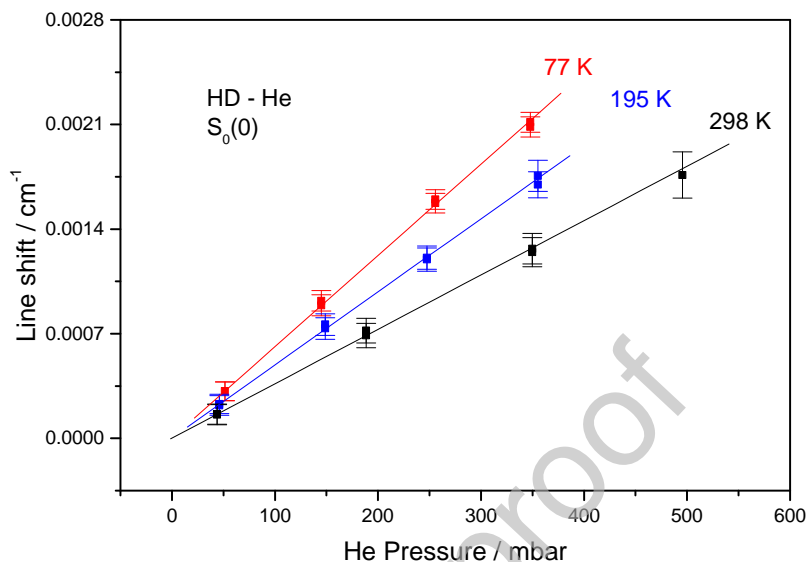


Figure 10: (Color online) Experimental line-shifts of the  $S_0(0)$  line at 77 K (red dots), 195 K (blue dots) and 298 K (black dots) and linear fits (lines in red, blue and black) for the three temperatures.

obtained coefficients for all lines and temperatures are displayed in Table 4.

## 350 6. The collisional line-shape effects and comparison between theory and experiment

In this section we show that, in order to properly interpret experimental data and compare with the results of the *ab initio* quantum scattering calculations, the beyond-Voigt line-shape effects have to be taken into account. In this respect, any molecular hydrogen isotopologue is very atypical and exhibits strong  
 355 speed dependence (SD) of collisional broadening and shift as well as a very pronounced influence of the velocity-changing (VC) collisions. In Section 6.1, we discuss the line-shape effects relevant for the considered here He-perturbed HD pure rotational lines. These lines exhibit even more interesting collisional  
 360 effects than other molecular hydrogen spectra, because here not only the SD of broadening and shift are very strong, but also the SD of broadening is much

larger than the SD of shifting, which results in enhancement of the inhomogeneous collisional asymmetry, see Section 6.2. In Section 6.3, we compare our full theoretical results with experiment.

### 365 6.1. The collisional line-shape effects

In the case of molecular hydrogen spectra, the beyond-Voigt line-shape effects are atypically pronounced. Besides the basic Lorentzian broadening,  $\gamma_0$ , and shift,  $\delta_0$ , parameters, one has to consider their SD and the VC collisions. We tested that the present state-of-the-art approaches (Wcisło et al. 2018) incorporating the exact form of *ab initio* SD and billiard-ball (Ciuryło et al. 2001) or Blackmore (Wciso and Ciuryo 2013) models of VC collisions lead only to small corrections comparing simpler approximated methods at present conditions (high-pressure limit) and experimental accuracy. Therefore, it suffices to use a model based on a quadratic approximation of SD and hard-collision approximation of the VC collisions. The resulting profile is called SD hard-collisions profile with quadratic SD ( $SD_qHCP$ ). The SD of broadening and shift is quantified by  $\gamma_2$  and  $\delta_2$  parameters. The real and imaginary rates of the VC collisions are denoted by  $\tilde{\nu}_{opt}^r$  and  $\tilde{\nu}_{opt}^i$  (Eq. (9)). Therefore,  $SD_qHCP$  is parametrized by six collisional line-shape parameters:  $\gamma_0$ ,  $\delta_0$ ,  $\gamma_2$ ,  $\delta_2$ ,  $\tilde{\nu}_{opt}^r$  and  $\tilde{\nu}_{opt}^i$ ; all of them are determined from our *ab initio* quantum scattering calculations (Wcisło et al. 2018), see Eqs. (6) and (9). The definition of  $\gamma_2$  and  $\delta_2$  can be found in Tennyson and et al. (2014); Stolarczyk et al. (2019), Kowzan et al.

The influence of the beyond-Voigt line-shape effects on the spectra considered here are shown in Fig. 11 for the case of  $S_0(2)$  line in He-perturbed HD at  $T = 298$  K in the high-pressure regime where the Doppler effect is completely washed out by the Dicke narrowing. The green line is the full  $SD_qHCP$  with *ab initio* values of six collisional line-shape parameters:  $\gamma_0 = 8.46$ ,  $\delta_0 = 3.64$ ,  $\gamma_2 = 3.60$ ,  $\delta_2 = 1.54$ ,  $\tilde{\nu}_{opt}^r = 28.8$  and  $\tilde{\nu}_{opt}^i = -1.84$  (all the numbers are in the unit of  $10^{-3} \text{ cm}^{-1}/\text{amg}$ ). The gray line is a Lorentz profile with *ab initio*  $\gamma_0$  and  $\delta_0$  (the same as the aforementioned ones for  $SD_qHCP$ ). The SD of broadening and shift leads to inhomogeneous collisional narrowing and broadening of the

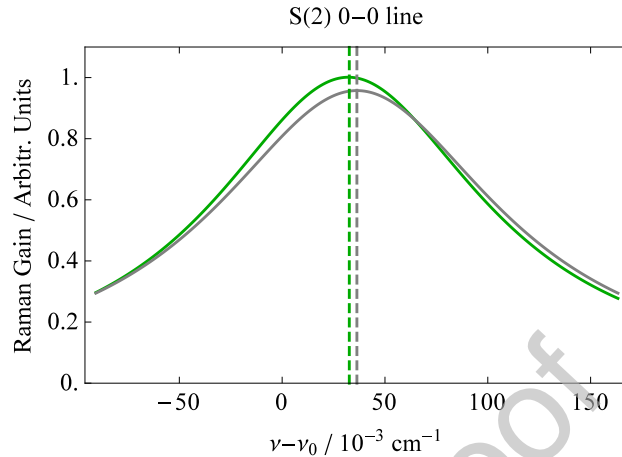


Figure 11: (Color online) Comparison of the full  $SD_qHC$  profile (green line) with the simple Lorentz profile (gray line) for the  $S_0(2)$  line in He-perturbed HD at  $T = 298$  K. The comparison is done for the high-pressure limit,  $n = 10$  amg, where the Doppler component is completely negligible. For the Lorentz profile we used our *ab initio* broadening,  $\gamma_0$ , and shift,  $\delta_0$ , parameters, while for the  $SD_qHC$  profile we used the full set of the *ab initio* line-shape parameters:  $\gamma_0$ ,  $\delta_0$ ,  $\gamma_2$ ,  $\delta_2$ ,  $\tilde{\nu}_{opt}^r$  and  $\tilde{\nu}_{opt}^l$ . The green and gray vertical dashed lines are the effective positions of the  $SD_qHC$  and Lorentz profiles; the difference of the pressure shifts originates from the nonzero value of the  $\delta_2$  parameter and the asymmetry enhancement effects caused by  $\gamma_2$ , see Section 6.2. The  $SD_qHC$  profile is narrower than the Lorentzian, because the speed-dependent effect is dominated by the speed-dependence of broadening ( $\gamma_2 > \delta_2$ ).

profile, respectively. Since  $\gamma_2$  is much larger than  $\delta_2$ , the  $SD_qHCP$  is effectively narrower than the Lorentzian, see Fig. 11; see also the comparison between the gray and green lines in upper panels in Fig. 12.

### 395 6.2. Enhancement of the collisional inhomogeneous line asymmetry

In the simple case of a Voigt profile the effective position of the molecular line is given by a sum of its unperturbed line position and the collisional shift,  $\nu_0 + p\delta_0$ . However, when the collisional shift depends on the speed of an active molecule, i.e.  $\delta_2 \neq 0$ , then the line is additionally broadened and asymmetric (this contribution is called inhomogeneous collisional broadening). The  
400 asymmetric (this contribution is called inhomogeneous collisional broadening). The asymmetry causes that the effective position of the line is additionally shifted.

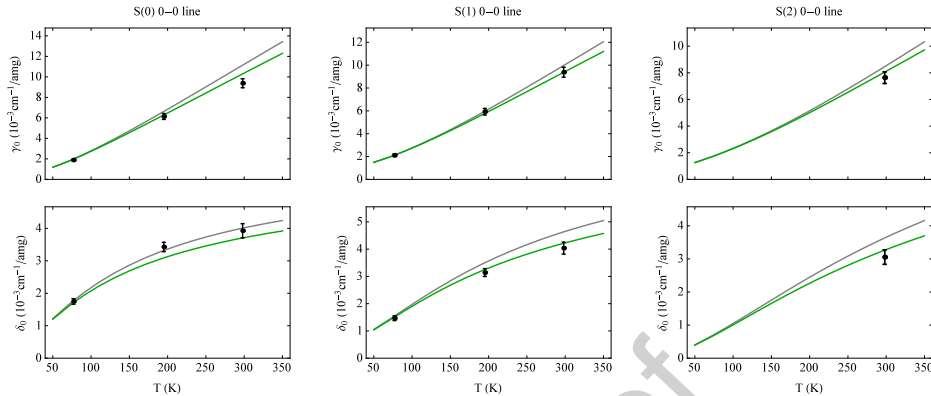


Figure 12: (Color online) Comparison of our experimental results and *ab initio* calculations for the pure rotational S lines in He-perturbed HD. The black points are the experimental shifts and half-widths at half maximum determined by fitting the actual experimental spectra with Voigt profile and extrapolating the fitted values of  $\gamma_0$  and  $\delta_0$  parameters to the high-pressure limit, see Section 5 for details. The gray lines are the direct values of the  $\gamma_0$  and  $\delta_0$  parameters from our *ab initio* calculations, see Eq. (6). The green lines are the effective width and shift of the  $SD_qHC$  that we expect to observe in experiment determined as shown in Fig. 13. The experimental black points should be compared with green lines.

However, since for molecular hydrogen the real part of the frequency of the VC collisions,  $\tilde{\nu}_{opt}^r$ , is large, the inhomogeneous asymmetry and its associated additional shift are (strongly) reduced. This competition between SD effects and VC collisions is well known in molecular hydrogen spectra analysis (Wcisło et al. 2015). For most cases of self- and foreign-perturbed molecular hydrogen lines, the above described picture is valid, for instance see Wcisło et al. (2015) for Ar-perturbed  $H_2$  Q(1) 1-0 line, Wcisło et al. (2018) for self-perturbed  $D_2$  S(2) 2-0 line and Slowinski et al. for He-perturbed  $H_2$  2-0 Q(1) and 3-0 S(1) lines. The system considered in this article is atypical and exhibits intriguing features. Indeed, in the present case the SD effects are not dominated by the SD of the shift, but by the SD of the broadening. The obvious consequence is that SD effects effectively lead to narrowing of the profile, for example see Fig. 11 for the He-perturbed HD  $S_0(2)$  line (the green line including SD effects is clearly narrower than its Lorentzian counterpart). This narrowing is also seen

in the upper panels in Figs. 12 and B.1. The intriguing feature that we observed here is not related to the widths of the lines, but to their effective shifts. If we simulate the  $SD_qHC$  profile without the SD of broadening ( $\gamma_2 = 0$ ) then the effective line shift is very close to  $\delta_0$  (in such case the two vertical lines from Fig. 11 would overlap). This is caused by the fact that  $\tilde{\nu}_{opt}^r$  is much larger than  $\delta_2$  and the  $\delta_2$ -induced asymmetry of the line is completely unobservable because of the much more pronounced influence of VC collisions. The intriguing feature is that if we turn on the SD of broadening (i.e., we set  $\gamma_2$  to its value deduced from our *ab initio* speed dependent broadening coefficients) then the line gets asymmetric and hence effectively shifted, see Fig. 11. This behavior is quite unexpected because, due to the symmetry of the line-shape equations,  $\gamma_2$  by itself cannot induce any asymmetry of the line. To ensure that this is a physical effect and not caused by the simplifications assumed in the  $SD_qHC$  model or by some numerical problems related to the used computer algorithm, we repeated these simulations with a much more sophisticated line-shape model (a speed dependent billiard-ball model with *ab initio* speed dependence (Ciuryło et al. 2001) based on completely different numerical algorithms (Wcisło et al. 2013)) reaching exactly the same conclusion. Our interpretation of this effect is that although the SD of broadening cannot induce line asymmetry by itself, it enhances the contribution of the SD line shift within the competition between the SD of line shift and VC collisions. It should be emphasized that the differences between effective line shifts of  $SD_qHC$  and Lorentzian models from Fig. 11 and lower panels in Figs. 12 are completely caused by this enhancement effect and without it the gray and green lines from these figures would be overlapped.

### 6.3. Comparison between theory and experiment

The comparison of our experimental results and *ab initio* calculations for the pure rotational S lines in He-perturbed HD is shown graphically in Fig. 12. The black points are the experimental shifts and half-widths at half maximum determined by fitting the actual experimental spectra with a Voigt profile and extrapolating the fitted values of  $\gamma_0$  and  $\delta_0$  parameters to the high-pressure

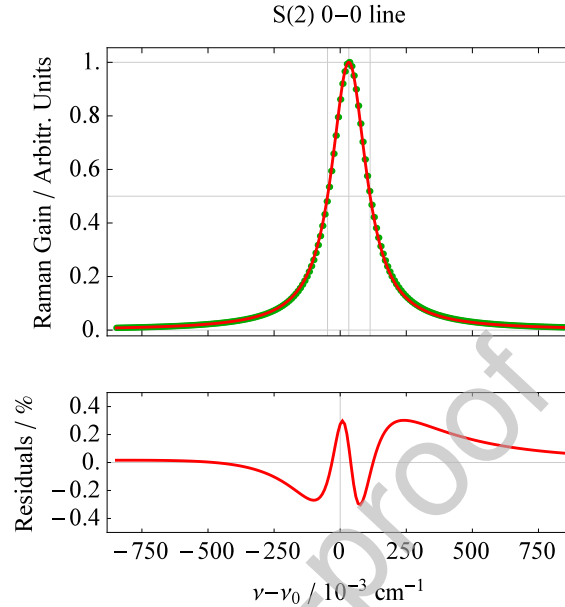


Figure 13: (Color online) Lorentzian fit to the *ab initio*  $\text{SD}_q\text{HC}$  profile for the  $\text{S}_0(2)$  line in He-perturbed HD. The green points represent the *ab initio*  $\text{SD}_q\text{HC}$  profile; exactly the same as the green line in Fig. 11, i.e., generated for  $T = 298 \text{ K}$  and  $n = 10 \text{ amg}$ . The red line is a Lorentzian fit, whose broadening,  $\gamma_0$ , and shift,  $\delta_0$ , parameters quantify the effective width and shift of our *ab initio*  $\text{SD}_q\text{HC}$  profile. This is the way how the green lines from Figs. 12 and B.1 were determined.

limit, see Section 5 for details. The error bars are  $1 \sigma$  standard errors. The gray lines from Fig. 12 are the direct values of the  $\gamma_0$  and  $\delta_0$  parameters from our *ab initio* calculations, see Eq. (6). The green lines in Fig. 12 are the effective widths and shifts of the *ab initio*  $\text{SD}_q\text{HC}$  model. In Fig. 13, we demonstrate the procedure we used to determine them. The green points in Fig. 13 represent our *ab initio*  $\text{SD}_q\text{HCP}$  and the red line is a Lorentzian fit. The bottom panel of Fig. 13 shows the residuals from the fit. The fitted values of the Lorentzian  $\gamma_0$  and  $\delta_0$  give us information about effective half-width at half-maximum and shift of the line that we expect to observe in the experiment. The values of these two fitted parameters are shown in Fig. 12 (green lines) as a function of temperature. Our experimental data (black points in Fig. 12) should be compared with the

green lines. It is seen that for almost all the cases from Fig. 12 the green lines agree with experiment within combined experimental and theoretical  $1 \sigma$  (we estimate theoretical uncertainty at 2.5 % (Jwiak et al. 2018)), which is not the case for the gray line. The data provided by our  $SD_qHCP$  analysis are also reported in Tables 3 and 4. This demonstrates that the incorporation of the collisional line-shape effects is necessary for a proper physical interpretation of the experimental data.

In the Appendix B we show a similar comparison, but for R lines.

## 7. Conclusion

In this article, using the most recent and expected most accurate *ab initio* PES of Thibault et al. (2017) for  $H_2$ -He, we have presented line-shape parameters for the purely rotational dipole  $R_0(j=0-3)$  and Raman  $S_0(j=0-2)$  lines of HD in helium baths. Our values compare very well with previous calculations performed for the  $R_0(j=0-1)$  (Green 1974; Schaefer and Monchick 1987, 1992; Gustafsson and Frommhold 2001a) and  $S_0(j=0)$  (Green 1974) lines. However, there is still a quite large disagreement with available experimental data existing for the R lines (Drakopoulos and Tabisz 1987; Ulivi et al. 1989; Lu et al. 1993). Therefore, new measurements performed at atmospheres-relevant densities would be welcome for these lines of astrophysical and atmospherical interest.

A simple Voigt profile is inadequate to simulate such spectra and capture their complexity. By using a speed dependent hard collision profile, we show that not only effects coming from internal changes due to collisions must be considered to reach good agreement between experimental and calculated data but also effects coming from the translational motion and the correlations between these different kinds of phenomena. Taking into account these effects we obtained very good agreement between our theoretical data and the ones deduced from our SRS measurements.

In addition, we provide as supplementary material (Thibault et al. 2019) a

first complete set of line shape parameters for purely rotational electric dipole and Raman lines. This includes for the  $R_0(j=0-3)$  and  $S_0(j=0-2)$  the various cross sections, the  $\Omega$  integrals, GHM parameters, the speed dependence of the line shape parameters as well as thermally averaged values between 10 and 500  
 490 K. Thus our data set is well suited to generate from a simple Voigt to the most elaborated line profiles including effects arising from internal changes and the translational motion.

### Acknowledgements

RZM and DB acknowledge the funding received from Project FIS2017-84391-  
 495 C2-1-P of Ministerio de Economía y Competitividad. PW contribution is supported by the National Science Centre in Poland through Projects Nos. 2015/19/D/ST2/02195 and 2018/31/B/ST2/00720. The project is cofinanced by the Polish National Agency for Academic Exchange under the PHC Polonium program (dec. PPN/X/PS/318/2018). PW and FT are supported by the French-Polish PHC Polonium program (project  
 500 42769ZK for the French part).

### Appendix A. Relation between the Dicke parameter $\nu_{opt}$ for the velocity changing collisions and the empirical one $\nu_{diff}$

When one wants to consider the effect of the velocity changing collisions on the line shape, as an initial value in a line fitting procedure or by default, the  
 505 frequency of such collisions is often fixed to  $\nu_{diff}$  (Hartmann et al. 2008) which is deduced from the mass diffusion coefficient  $D_{ab}$  (Hirschfelder et al. 1967) via:

$$\nu_{diff} = \frac{k_B T}{m_a D_{ab}}, \quad (\text{A.1})$$

where  $m_a$  is the mass of the optically active molecule. The cross section  $\sigma_1^q$  that allows the determination of the  $\omega_1^{1,1}(q)$  collision integral has no classical equivalent. However, it can be demonstrated that for structureless colliding particles,  
 510 thus driven by one and only one central potential, the real part of that cross section reduces to a momentum-transfer cross section (see also the discussions

in the appendices A and B of Thibault et al. (2017) and in the supplementary material of Martínez et al. (2018)). Therefore the important difference between the frequency of the velocity changing collisions derived from the diffusional motion and the complex Dicke parameter  $\nu_{opt}$ , as given by Eq. (9), is that the latter includes the transport of the internal polarization and thus depends on the rovibrational transition.

In our previous works about H<sub>2</sub>-He (Thibault et al. 2017) and D<sub>2</sub>-He Martínez et al. (2018) we have shown that the effective parameter  $\nu_{diff}$  and the true frequency of the VC collisions  $\nu_{opt}$  are very close because of the great importance of the isotropic interaction as compared to the anisotropic components (starting with  $L = 2$ ) and the weakness of the inelastic collisions, at least up to room temperature. Figure A.1 shows the same comparison for the R<sub>0</sub>(0) and S<sub>0</sub>(2) lines in helium. The classical value for  $\nu_{diff}$  has been obtained following Hirschfelder et al. (1967) performing simple classical calculations on the isotropic term of the HD-He PES. The close coupling method allows the distinction of the frequency of the VC collisions, even if it is small, for the two different lines. This appears naturally within the GHM. The value deduced from our classical method is not bad but insufficient for an accurate line shape analysis. The difference increases with temperature, which we may relate with the increase of the inelastic collisions. As compared to the previous studied systems (Thibault et al. 2017; Martínez et al. 2018) the difference is bigger between  $\nu_{diff}$  and  $\nu_{opt}$  because of the lack of symmetry (the PES include odd anisotropic components). Finally, let us note that this difference is even bigger for CO in Ar baths because of the predominance of the inelastic collisions for this system Kowzan et al.

## Appendix B. Line-shape analysis for R lines

In this appendix we graphically show (Fig. B.1) the results of our quadratic speed dependent hard collision profile (SD<sub>q</sub>HC) for the studied R lines, exactly as it has been performed for the S lines, see Section 6. The meaning of the gray and green lines is exactly the same as in Fig. 12. The experimental data (black

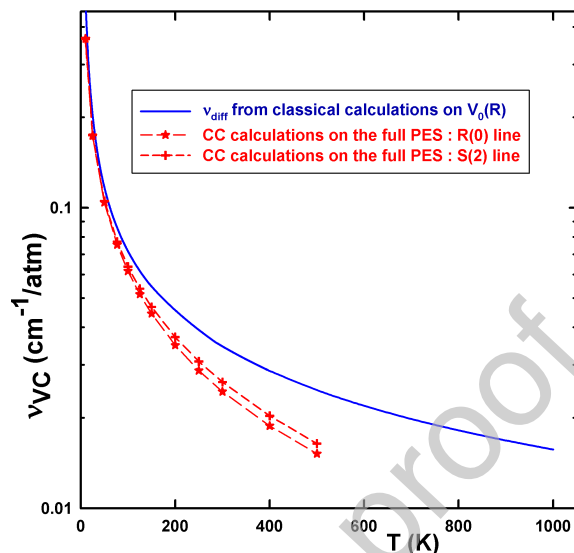


Figure A.1: (Color online) Comparison of the frequency of the VC collisions (in  $\text{cm}^{-1}/\text{atm}$ ) obtained with the GHM,  $\nu_{opt}$ , with the diffusional frequency  $\nu_{diff}$  at various temperatures.

points) are taken from Drakopoulos and Tabisz (1987), Ulivi et al. (1989), and Lu et al. (1993). The observed halfwidths and shifts should be slightly smaller than the collisional parameters  $\gamma_0$  and  $\delta_0$  as shown by the green lines. The values deduced from our  $\text{SD}_q\text{HCP}$  analysis at 77, 195 and 296 K are also reported in  
 545 Tables 1 and 2. We also observe more important disagreement between our values deduced from our line-shape analysis ( $\text{SD}_q\text{HC}$ ) and the experimental values than between our comparisons for S lines. Thus new experiments for pure rotational R lines should be undertaken.

### Data Availability

550 Datasets related to this article can be found at :  
<https://data.mendeley.com/datasets/32jjp9fmgc/draft?a=514c796e-235e-482d-9b8f-2d670dc8fc1c>  
 Mendeley Data, v1 <http://dx.doi.org/10.17632/32jjp9fmgc.1>

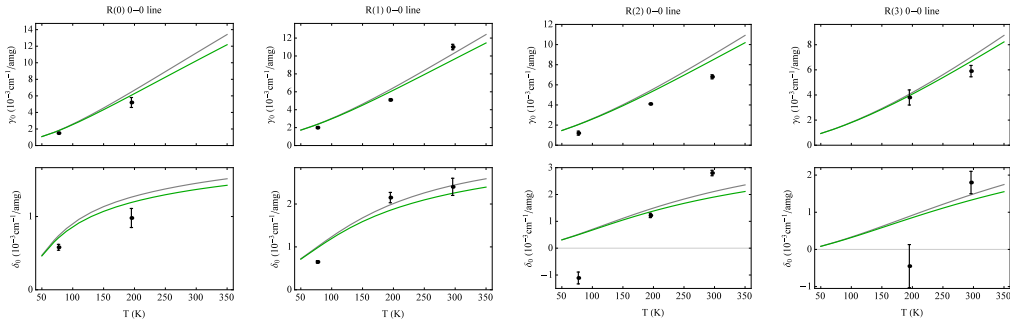


Figure B.1: (Color online) Comparison of experimental results and our *ab initio* calculations for the first pure rotational R lines in He-perturbed HD. The black points are the experimental shifts and half-widths at half maximum taken from Drakopoulos and Tabisz (1987); Ulivi et al. (1989); Lu et al. (1993). The gray lines are the direct values of the  $\gamma_0$  and  $\delta_0$  parameters from our *ab initio* calculations, see Eq. (6). The green lines are the effective width and shift of the  $SD_qHC$  that we expect to observe in experiment determined as shown in Fig. 13. The experimental black points should be compared with green lines.

Associated reference in the main text : Thibault et al. (2019).

#### 555 Declaration of interests

The authors declare that they have no known competing financial interests or personal relationships that could have appeared to influence the work reported in this paper.

#### References

- 560 Alexander, M. H., Manolopoulos, D. E., 1987. A stable linear reference potential algorithm for solution of the quantum closecoupled equations in molecular scattering theory. *The Journal of Chemical Physics* 86 (4), 2044–2050.
- Altwegg, K., Balsiger, H., Bar-Nun, A., Berthelier, J. J., Bieler, A., Bochsler, P., Briois, C., Calmonte, U., Combi, M., De Keyser, J., Eberhardt, P., Fiethe, B., Fuselier, S., Gasc, S., Gombosi, T. I., Hansen, K., Hässig, M., Jäckel, A.,  
565 Kopp, E., Korth, A., LeRoy, L., Mall, U., Marty, B., Mousis, O., Neefs, E.,

- Owen, T., Rème, H., Rubin, M., Sémon, T., Tzou, C.-Y., Waite, H., Wurz, P., 2015. 67P/Churyumov-Gerasimenko, a Jupiter family comet with a high D/H ratio. *Science* 347 (6220).
- 570 Bakr, B. W., Smith, D. G. A., Patkowski, K., 2013. Highly accurate potential energy surface for the He-H<sub>2</sub> dimer. *J Chem Phys* 139, 144305.
- Baranger, M., 1958a. Simplified quantum-mechanical theory of pressure broadening. *Phys Rev* 111, 481–493.
- Baranger, M., 1958b. Problem of overlapping lines in the theory of pressure  
575 broadening. *Phys Rev* 111, 494–304.
- Baranger, M., 1958c. General impact theory of pressure broadening. *Phys Rev* 112, 855–865.
- Ben-Reuven, A., 1966a. Symmetry considerations in pressure-broadening theory. *Phys Rev* 141, 34–40.
- 580 Ben-Reuven, A., 1966b. Impact broadening of microwave spectra. *Phys Rev* 145, 7–22.
- Blackmore, R., 1987. A modified Boltzmann kinetic equation for line shape functions. *The Journal of Chemical Physics* 87 (2), 791–800.
- Ciuryło, R., Shapiro, D. A., Drummond, J. R., May, A. D., Dec 2001. Solving  
585 the line-shape problem with speed-dependent broadening and shifting and with Dicke narrowing. II. application. *Phys. Rev. A* 65, 012502.
- Corey, G. C., McCourt, F. R., 1984. Dicke narrowing and collisional broadening of spectral lines in dilute molecular gases. *J Chem Phys* 81, 2318–2329.
- Cozijn, F. M. J., Dupré, P., Salumbides, E. J., Eikema, K. S. E., Ubachs, W.,  
590 Apr 2018. Sub-Doppler frequency metrology in HD for tests of fundamental physics. *Phys. Rev. Lett.* 120, 153002.

- Demeio, L., Green, S., Monchick, L., 1995. Effects of velocity changing collisions on line shapes of HF in Ar. *J Chem Phys* 102, 9160–9166.
- Drakopoulos, P. G., Tabisz, G. C., Dec 1987. Collisional interference in the  
595 foreign-gas-perturbed far-infrared rotational spectrum of HD. *Phys. Rev. A* 36, 5566–5574.
- Dubernet, M.-L., Tuckey, P., 1999. Raman Q and S line broadening and shifting coefficients: some commonly used assumptions revisited. *Chemical Physics Letters* 300 (3), 275–280.
- 600 Encrenaz, T., Bibring, J.-P., Blanc, M., Barucci, M.-A., Roques, F., Zarka, P., 2004. *The Solar System*. Springer-Verlag Berlin Heidelberg.
- Fano, U., 1963. Pressure broadening as a prototype of relaxation. *Phys Rev* 131, 259–268.
- Fasci, E., Castrillo, A., Dinesan, H., Gravina, S., Moretti, L., Gianfrani, L., Aug  
605 2018. Precision spectroscopy of HD at 1.38  $\mu\text{m}$ . *Phys. Rev. A* 98, 022516.
- Feuchtgruber, H., Lellouch, E., Orton, G., de Graauw, T., Vandenbussche, B., Swinyard, B., Moreno, R., Jarchow, C., Billebaud, F., Cavalié, T., Sidher, S., Hartogh, P., 2013. The D/H ratio in the atmospheres of Uranus and Neptune from Herschel-PACS observations. *A&A* 551, A126.
- 610 Garberoglio, G., Patkowski, K., Harvey, A. H., 2014. Fully quantum cross second virial coefficients for the three-dimensional He-H<sub>2</sub> pair. *Int J Thermophys* 35, 1435–1449.
- Green, S., 1974. Rotational excitation of HD by collisions with He. *Physica* 76 (3), 609–615.
- 615 Green, S., Liu, W.-K., McCourt, F., 1983. Close-coupled calculations of viscosity transport-relaxation cross sections for HD-He: Comparison with experiment. *Physica A: Statistical Mechanics and its Applications* 117 (2), 616–630.

- Gustafsson, M., Frommhold, L., 2001a. The HD-He complex: Interaction-induced dipole surface and infrared absorption spectra. *The Journal of Chemical Physics* 115 (12), 5427–5432. 620
- Gustafsson, M., Frommhold, L., Apr 2001b. Intracollisional interference of R lines of HD in mixtures of deuterium hydride and helium gas. *Phys. Rev. A* 63, 052514.
- Hartmann, J.-M., Boulet, C., Robert, D., 2008. *Collisional Effects on Molecular Spectra*. Elsevier, Amsterdam. 625
- Hartmann, J.-M., Tran, H., Armante, R., Boulet, C., Campargue, A., Forget, F., Gianfrani, L., Gordon, I., Guerlet, S., Gustafsson, M., Hodges, J. T., Kassi, S., Lisak, D., Thibault, F., Toon, G. C., 2018. Recent advances in collisional effects on spectra of molecular gases and their practical consequences. *Journal of Quantitative Spectroscopy and Radiative Transfer* 213, 178–227. 630
- Hess, S., 1972. Kinetic theory of spectral line shapes. the transition between Doppler broadening and collisional broadening. *Physica* 61, 80–94.
- Hirschfelder, J. O., Curtiss, C. F., Bird, R. B., 1967. *Molecular Theory of Gases and Liquids*. 4th ed. Wiley, New York.
- Hutson, J. M., Green, S., 1995. Molscat version14, Collaborative Computational Project 6 of the UK Science and Engineering Research Council, Daresbury Laboratory, UK. 635
- Jwiak, H., Thibault, F., Stolarczyk, N., Wciso, P., 2018. Ab initio line-shape calculations for the S and O branches of H<sub>2</sub> perturbed by He. *Journal of Quantitative Spectroscopy and Radiative Transfer* 219, 313–322. 640
- Kassi, S., Campargue, A., 05 2011. Electric quadrupole and dipole transitions of the first overtone band of HD by CRDS between 1.45 and 1.33  $\mu\text{m}$ . *Journal of Molecular Spectroscopy* 267, 36–42.

- Kowzan, G., Wcisło, P., Slowinski, M., Masłowski, P., Viel, A., Thibault,  
645 F., ????. Fully quantum calculations of the line-shape parameters for the  
Hartmann-Tran profile: a CO-Ar case study. submitted to JQSRT.
- Lellouch, E., Bézard, B., Fouchet, T., Feuchtgruber, H., Encrenaz, T.,  
de Graauw, T., 2001. The deuterium abundance in Jupiter and Saturn from  
ISO-SWS observations. *A&A* 370 (2), 610–622.
- 650 Lu, Z., Tabisz, G. C., Ulivi, L., Feb 1993. Temperature dependence of the pure  
rotational band of HD: Interference, widths, and shifts. *Phys. Rev. A* 47,  
1159–1173.
- Martínez, R. Z., Bermejo, D., Thibault, F., Wcisło, P., 2018. Testing the ab  
initio quantum-scattering calculations for the D<sub>2</sub>-He benchmark system with  
655 stimulated Raman spectroscopy. *J Raman Spectrosc* 49, 1339–1349.
- McCourt, F. R. W., Weir, D., Thachuk, M., Clark, G. B., 2005. Transport  
and relaxation properties of isotopomeric hydrogenhelium binary mixtures.  
II. HD, D<sub>2</sub>, T<sub>2</sub>He mixtures. *Molecular Physics* 103 (1), 45–58.
- Menten, K. M., Wyrowski, F., 2011. Molecules detected in interstellar space.  
660 *Interstellar Molecules*, K. M. T. Yamada and G. Winnewisser (eds.), Springer  
Tracts in Modern Physics Springer-Verlag Berlin Heidelberg 241.
- Monchick, L., Hunter, L. W., 1986. Diatomic-diatom molecular collision inte-  
grals for pressure broadening and Dicke narrowing: A generalization of Hess's  
theory. *J Chem Phys* 85, 713–718.
- 665 Muchnick, P., Russek, A., 1994. The HeH<sub>2</sub> energy surface. *J Chem Phys* 100,  
4336–4346.
- Nolte, J. L., Stancil, P. C., Lee, T.-G., Balakrishnan, N., Forrey, R. C., dec  
2011. Rovibrational quenching rate coefficients of HD in collisions with He.  
*The Astrophysical Journal* 744 (1), 62.

- 670 Pachucki, K., Komasa, J., Nov 2008. Electric dipole rovibrational transitions in  
the HD molecule. *Phys. Rev. A* 78, 052503.
- Pachucki, K., Komasa, J., 2010. Rovibrational levels of HD. *Phys. Chem. Chem.  
Phys.* 12, 9188–9196.
- Pine, A. S., 1999. Asymmetries and correlations in speed-dependent Dicke-  
675 narrowed line shapes of argon-broadened HF. *J Quant Spectrosc Radiat  
Transfer* 62, 397–423.
- Salumbides, E. J., Koelemeij, J. C. J., Komasa, J., Pachucki, K., Eikema, K.  
S. E., Ubachs, W., Jun 2013. Bounds on fifth forces from precision measure-  
ments on molecules. *Phys. Rev. D* 87, 112008.
- 680 Schaefer, J., Monchick, L., 1987. Line shape cross sections of HD immersed  
in He and H<sub>2</sub> gas. I. Pressure broadening cross sections. *J Chem Phys* 87,  
171–181.
- Schaefer, J., Monchick, L., 1992. Line broadening of HD immersed in He and  
H<sub>2</sub> gas. *A&A* 265, 859–868.
- 685 Shafer, R., Gordon, R. G., 1973. Quantum scattering theory of rotational re-  
laxation and spectral line shapes in H<sub>2</sub> - He gas mixtures. *J Chem Phys* 58,  
5422–5443.
- Slowinski, M., Thibault, F., Tan, Y., Wang, J., Liu, A.-W., Hu, S.-M., Kassi,  
S., Campargue, A., Konefal, M., Jozwiak, H., Patkowski, K., Żuchowski, P.,  
690 Ciuryło, R., Lisak, D., Wcisło, P., 0000. Spectroscopic studies of the H<sub>2</sub>-He  
collisions. Unpublished results.
- Sprecher, D., Liu, J., Jungen, C., Ubachs, W., Merkt, F., 2010. Communication:  
The ionization and dissociation energies of HD. *The Journal of Chemical  
Physics* 133 (11), 111102.
- 695 Stolarczyk, N., Thibault, F., Cybulski, H., Jwiak, H., Kowzan, G., Vispoel, B.,  
Gordon, I., Rothman, L., Gamache, R., Wcisło, P., 2019. Evaluation of differ-

- ent parameterizations of temperature dependences of the line-shape parameters based on ab initio calculations: case study for the HITRAN database. *Journal of Quantitative Spectroscopy and Radiative Transfer*, 106676.
- 700 Tabisz, G. C., 2003. Interference effects in the infrared spectrum of HD; Atmospheric implications. In "Weakly Interacting Molecular Pairs: Unconventional Absorbers of Radiation in the Atmosphere. Vol. 83-92. C. Camy-Peyret and A.A. Vigasin (eds.), Kluwer Academic Publishers.
- Tao, L.-G., Liu, A.-W., Pachucki, K., Komasa, J., Sun, Y. R., Wang, J., Hu, 705 S.-M., Apr 2018. Toward a determination of the proton-electron mass ratio from the Lamb-Dip measurement of HD. *Phys. Rev. Lett.* 120, 153001.
- Tennyson, J., 2003. *Molecules in Space: in Handbook of Molecular Physics and Quantum Chemistry*. Edited by Stephen Wilson, John Wiley & Sons, Ltd, Chichester.
- 710 Tennyson, J., et al., 2014. Recommended isolated-line profile for representing high-resolution spectroscopic transitions (IUPAC Technical Report). *Pure Appl Chem* 86, 1931–1943.
- Thibault, F., Martinez, R. Z., Bermejo, D., Wcisło, P., 2019. HD in He generalized cross sections. Mendeley data.
- 715 Thibault, F., Patkowski, K., Zuchowski, P., Józwiak, H., Wcisło, P., Ciuryło, R., 2017. Rovibrational line-shape parameters for H<sub>2</sub> in He and new H<sub>2</sub>-He potential energy surface. *J Quant Spectrosc Radiat Transfer* 202, 308–320.
- Thibault, F., Wcisło, P., Ciuryło, R., 2016. A test of H<sub>2</sub>-He potential energy surfaces. *EPJD* 70, 236.
- 720 Ubachs, W., Koelemeij, J., Eikema, K., Salumbides, E., 2016. Physics beyond the standard model from hydrogen spectroscopy. *Journal of Molecular Spectroscopy* 320, 1 – 12.

- Ulivi, L., Lu, Z., Tabisz, G. C., Jul 1989. Temperature dependence of the collisional interference in the pure rotational far-infrared spectrum of HD. Phys. Rev. A 40, 642–651. 725
- Wcisło, P., Cygan, A., Lisak, D., Ciuryło, R., Jul 2013. Iterative approach to line-shape calculations based on the transport-relaxation equation. Phys. Rev. A 88, 012517.
- Wcisło, P., Thibault, F., Cybulski, H., Ciuryło, R., May 2015. Strong competition between velocity-changing and phase- or state-changing collisions in H<sub>2</sub> spectra perturbed by Ar. Phys. Rev. A 91, 052505. 730
- Wcisło, P., Thibault, F., Zaborowski, M., Wójtewicz, S., Cygan, A., Kowzan, G., Masłowski, P., Komasa, J., Puchalski, M., Pachucki, K., Ciuryło, R., Lisak, D., 2018. Accurate deuterium spectroscopy for fundamental studies. J Quant Spectrosc Radiat Transfer 213, 41–51. 735
- Wciso, P., Ciuryo, R., 2013. Influence of the interaction potential shape on the Dicke narrowed spectral line profiles affected by speed-dependent collisional broadening and shifting. Journal of Quantitative Spectroscopy and Radiative Transfer 120, 36–43.
- 740 Zhou, B., Chen, M., 2017. Quantum rotational scattering of H<sub>2</sub> and its isotopologues with He. Molecular Physics 115 (19), 2442–2450.